Faraday Discussions

Accepted Manuscript

This manuscript will be presented and discussed at a forthcoming Faraday Discussion meeting. All delegates can contribute to the discussion which will be included in the final volume.

Register now to attend! Full details of all upcoming meetings: http://rsc.li/fd-upcoming-meetings

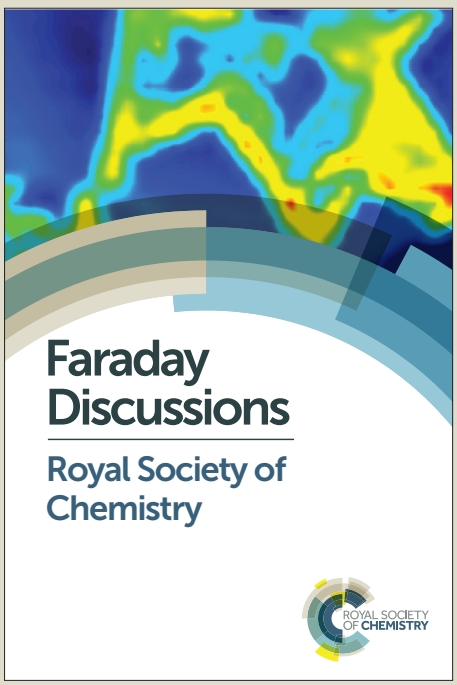

This is an *Accepted Manuscript*, which has been through the Royal Society of Chemistry peer review process and has been accepted for publication.

Accepted Manuscripts are published online shortly after acceptance, before technical editing, formatting and proof reading. Using this free service, authors can make their results available to the community, in citable form, before we publish the edited article. We will replace this *Accepted Manuscript* with the edited and formatted *Advance Article* as soon as it is available.

You can find more information about *Accepted Manuscripts* in the Information for Authors.

Please note that technical editing may introduce minor changes to the text and/or graphics, which may alter content. The journal's standard Terms & Conditions and the Ethical guidelines still apply. In no event shall the Royal Society of Chemistry be held responsible for any errors or omissions in this *Accepted Manuscript* or any consequences arising from the use of any information it contains.

ROYAL SOCIETY OF CHEMISTRY

www.rsc.org/faraday_d

CREATED USING THE RSC LaTeX PCCP ARTICLE TEMPLATE – SEE www.rsc.org/electronicfiles FOR DETAILS
PAPER www. rsc.org/faraday_d | Faraday Discussions

Coordination numbers and physical properties in molten salts and their mixtures

Dario Corradini,[a] Paul A. Madden[b] and Mathieu Salanne*[a]

Received Xth XXXXXXXXXX 20XX, Accepted Xth XXXXXXXXX 20XX
First published on the web Xth XXXXXXXXXX 200X
DOI: 10.1039/c000000x

Mixtures of trivalent metal halides with alkali halides are involved in many technologies but, from a more fundamental and general perspective, are worthy of study as interesting systems in which to examine the relationship between atomic-scale structure and physical properties. Here we examine the relationship between the viscosity and local and longer range structural measures in such mixtures where the trivalent metal cations span a significant size range and exhibit different behaviours in the dependence of their viscosity on the mixture composition. We characterise the structure and dynamics of the first coordination shell and the relationship between its structural relaxation time and the shear relaxation time of the mixture (the Maxwell relaxation time). We are then led to an examination of the structure of the networks which progressively form between the trivalent metal cations as their concentration increases in the mixtures. Here we find significant differences between small and larger cations, sufficient to explain the different behaviour of their viscosities. We draw attention to the similarities and differences of these networks which those which form in highly viscous, glass-forming materials like BeF_2:LiF.

1 Introduction

Molten salt mixtures play a central role in several emerging technologies, such as molten salt nuclear reactors[1] and pyroprocessing of nuclear waste[2–4], as well as in more established processes, like aluminium refinement[5]. Often the nature of the application involves extreme physical conditions, and the refinement of the selection of the salt requires knowledge and understanding of the way the physical properties respond to changes in composition, temperature etc. The accepted way to develop such understanding in modern liquid state science is via an appreciation of the link between atomic-scale structure and the properties of interest. Alongside the technological drive for designing suitable salts, "simple" inorganic molten salt mixtures have many favourable characteristics for pursuing the structure/property paradigm at a fundamental level - and in detail. Regarded as mixtures of spherical ions they are uncomplicated from the perspective of performing a range of directly interpretable experiments on structure. From a theo-

[a] *Sorbonne Universités, UPMC Univ Paris 06, CNRS, UMR 8234, PHENIX, F-75005, Paris, France; E-mail: mathieu.salanne@upmc.fr*
[n] *Department of Materials, University of Oxford, Parks Road, Oxford OX1 3PH, UK.*

retical perspective, many important materials, such as the halide melts of a wide range of technologically relevant trivalent cations can be accurately described on the basis of an ionic model [6,7] and, as we illustrate below, this can be used as the basis of simulation methods capable of accurately reproducing and predicting physical properties as well as structural information [8–13]. The structure/property relationship can then be explored via a detailed examination of the microscopic events in the simulation trajectory. In the ionic model, the most important parameter controlling the interionic interactions (and therefore, ultimately, the physical properties) is the ionic size, and a further attraction of the trivalent metals is that within the set of more than 20 elements forming trivalent cations with ionic halides there is a huge range of ionic sizes ranging from Al^{3+} to U^{3+} so that it becomes possible to rationalise the evolution of the behaviour of the physical properties across the whole set. We will focus on chloride melts in what follows, where most experiments and simulation studies have been focussed.

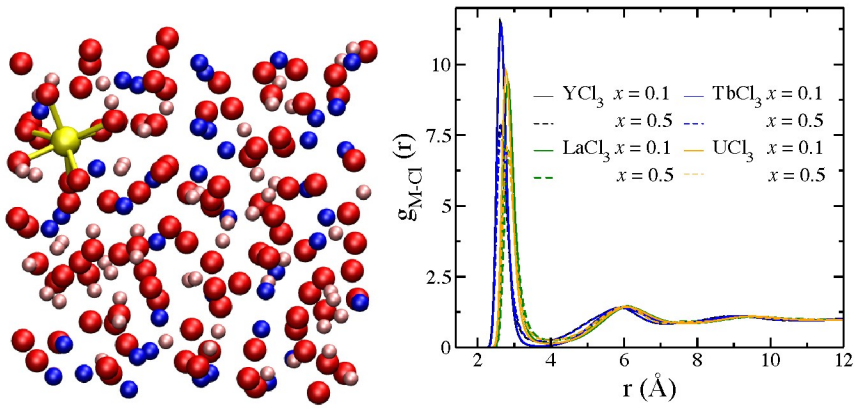

Fig. 1 Left: snapshot of a system consisting in one U^{3+} ion dissolved in the eutectic $(LiCl-KCl)_{eut}$ (blue: K^+, pink: Li^+, red: Cl^- and yellow: U^{3+}). The ionic bonds between the U and its first shell of Cl neighbors are shown with yellow sticks. Right: RDFs for the pairs $M^{3+}-Cl^-$ where M = Y, Tb, La and U at $T = 873$ K for two x_{MCl_3} mole fractions of MCl_3 in $(LiCl-KCl)_{eut}$.

It has been known for many years [14–16] that when trivalent metal cations are dissolved in halide melts they are surrounded by a tightly coordinated shell of anions, as illustrated in Figure 1. Although the experimental observables contain information about other structural features, a cornerstone of the traditional discussion of structure has been the coordination number, i.e. the number of anions in the coordination shell. In the crystalline state the coordination number is a well-defined quantity and in crystals of compounds of trivalent metal chlorides with alkali chlorides a coordination number of 6 around the trivalent cation is found across a very wide range cation sizes (i.e. octahedral coordination). When such compounds are melted, the Raman bands [17–19] associated with the vibrations of the coordination complex remain at close to the same frequency, even as the composition of the mixture is shifted towards the pure trivalent metal chloride, which suggests that octahedral coordination remains dominant in the melt. Early X-ray diffraction experiments on the melts of the pure materials were also

interpreted on the basis of a well-defined coordination number of 6, expected to persist across the composition range of mixtures[20]. More recent experimental and simulation studies have challenged this viewpoint. Neutron scattering allowed structure factors to be measured to much larger values of the scattering vector than could be achieved in the early X-ray measurements and hence allowed much better resolution of the full shape of the first peak of the M-Cl radial distribution function (RDF)[21–23] and thereby a more reliable value for the coordination number. The development of X-ray absorption fine structure measurements (EXAFS) on synchrotron sources allowed the structure around a particular cation to be measured even in relatively dilute solutions[13] where, previously, only the Raman observations had been possible. Finally, simulations have been refined to the point where, from a single simulation, the experimental data from all the experiments (X-ray [12], neutron[11], EXAFS[13], Raman [24]) performed on a given melt can be accurately reproduced giving the confidence that the uniquely detailed information available from an analysis of the ionic positions generated in the simulation trajectory is a faithful representation of the real material.

Such studies suggest a refinement of the traditional picture of a fixed coordination number. Firstly, in a melt the instantaneous coordination numbers around an ion take on a range of values around some preferred number[13,24]. For example, as discussed in reference 13, the instantaneous coordination number around a La^{3+} ion in a $(LiCl-KCl)_{eut}$ chloride melt ranges from 6 to 8 for a low mole fraction x_{LaCl_3}=0.01 and the experiment averages over their different contributions to the observable. Secondly, this distribution of instantaneous coordination numbers shifts with composition in mixtures, and in dilute solutions of a MCl_3 system in a weakly-coordinating alkali chloride the M^{3+} coordination does tend towards a well-defined value, in the sense that the distribution narrows around this value [13,24]. Furthermore, this dilute solution value is overwhelmingly likely to be 6 in chloride melts even across the very wide range of cation sizes in the set of interest. These realisations indicate that if we are to fulfil the objective of understanding the structure/property relationship in mixtures we will need to look well beyond the traditional mean coordination number measure of the former.

The picture which emerges of the ideal dilute solution then is of isolated octahedral coordination complexes around each M^{3+} cation floating in a sea of anions and alkali cations as illustrated in Figure 1. The cation could be regarded as having competed more strongly for the anions than the alkali cations and completed its ideal coordination structure. As the mixture becomes more concentrated this picture has to evolve; for example, beyond a composition of MCl_3:3AC, or $x_{MCl_3} = 0.25$ (A^+ represents an alkali cation), there are simply not enough chloride anions in the melt for isolated 6-coordinate clusters to form. Behaviour based on two extreme scenarios may follow, either the cation can reduce the number of anions in its coordination shell to remain isolated, or the individual cations might begin to share anions and have overlapping shells. There is good evidence to show that in the much studied case of cryolitic melts (AlF_3:NaF) the former happens[25–30] but for the chloride melts of principal interest to us, there is an increasing degree of corner and edge-sharing between coordination polyhedra as the MCl_3 concentration increases, leading ultimately to a network structure[13,24]. Rather than decreasing the coordination number this process leads to an increase in the mean coordination number for the larger cations, reaching 8 in

La^{3+}, for example. The rate at which this increase happens as the concentration changes depends on the identity of the alkali cation [13] as well as the M^{3+} ionic size, indicating that the tendency to corner or edge-share reflects a competition for coordination to the anions by the M^{3+} and alkali cations.

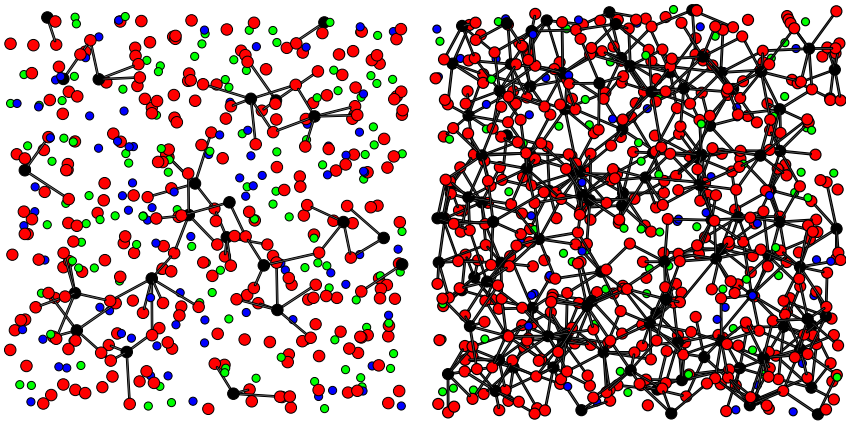

Fig. 2 Snapshots of a system consisting in $LaCl_3$ dissolved in the eutectic $(LiCl-KCl)_{eut}$ at two different concentrations (blue: K^+, green: Li^+, red: Cl^- and black: La^{3+}). The ionic bonds between the La and their first shells of Cl neighbors are shown with black sticks. Left: $x_{LaCl_3} = 0.1$, right: $x_{LaCl_3} = 0.5$.

In the remainder of this article we will illustrate the structure/property paradigm by showing how, just one physical property, the viscosity, is influenced by these factors affecting the structure of the melt as we vary its chemical composition. At the pictorial level, one can illustrate the origins of this connection by imagining a shear applied to the structures pictured in Figure 2 and trying to envisage how they will relax to a new configuration. This will involve some combination of a breaking or relative movement of the coordination complexes or, in the La picture, the stretching or breaking of the "bonds" which make up the network structure. The viscosity is an important physical property in some of the technologies mentioned at the outset. For example, in one design for a large scale molten salt reactor the liquid core is pumped at a very high rate to ensure, amongst other things, sufficiently rapid heat transfer. Clearly, it is vital to understand how the viscosity of the core would change as its composition is altered by the nuclear reaction or the addition of fresh fuel or by a change in temperature.

2 The simulations

We have conducted molecular dynamics simulations on mixtures composed of MCl_3 (where M^{3+} is Y^{3+}, Tb^{3+}, La^{3+}, U^{3+}) dissolved in $(LiCl–KCl)_{eut}$, at three temperatures: $T = 873$ K, $T = 973$ K and $T = 1073$ K. These cations span a range of ionic size which is of interest for the pyroprocessing studies (Y^{3+} 90.0 pm, Tb^{3+} 92.3 pm, La^{3+} 103.2 pm and U^{3+} 102.5 pm [31]), covering the rare earths as well as U^{3+}. The mole fraction of MCl_3 is varied from $x_{MCl_3} = 0$ to $x_{MCl_3} = 0.5$ in steps of $\delta x_{MCl_3} = 0.1$. The detailed composition of the examined systems is

summarized in Table 1. The eutectic composition (LiCl-KCl)$_{eut}$, $x_{LiCl} = 0.582$, is often chosen in experimental and technological studies because of its low melting point, $T_m^{eut} = 625$ K [32].

Table 1 Molecular composition of the considered systems for metal chloride mole fractions from $x_{MCl_3} = 0$ to $x_{MCl_3} = 0.5$. The ratio KCl/LiCl is approximately constant (0.712-0.720) and corresponding to the eutectic ratio (0.718) [32]. The total number of ions in the simulation box is also reported.

x_{MCl_3}	N_{MCl_3}	N_{LiCl}	N_{KCl}	N_{ions}
0.0	–	126	90	432
0.1	22	113	81	476
0.2	43	101	72	518
0.3	65	88	63	562
0.4	86	75	54	602
0.5	108	63	45	648

We use the polarizable ion model force field for performing our simulations [6,7]. In this model the ions carry their formal valence charges and the effect of the polarization of the anions by coulombic and short-range interactions with the cations is included. This has been shown to be essential to reproduce the experimental structural, thermodynamic and dynamical properties of the melts of interest. All the parameters of the force field are provided in reference 10. They have been validated in comparison with a wide range of experimentally obtained structural, thermodynamic and dynamical properties of these melts [10–13,33]. In particular, the activity coefficients of the trivalent ions of interest here were very successfully predicted by the simulations [10], as has recently been confirmed in a series of electrochemical measurements [34]. Some of these liquids have also been studied using potentials generated on a purely first-principles basis [35] with virtually identical results. Other details of the simulation methods are very similar to those reported in previous works [8–10,33].

3 Results

Viscosity

The shear viscosity is calculated from the integral over time of the autocorrelation function of the anisotropic elements of the stress tensor. This is known as Green-Kubo relation and it reads:

$$\eta = \frac{V}{k_B T} \int_0^\infty \left\langle \sigma_{\alpha\beta}(0)\sigma_{\alpha\beta}(t) \right\rangle \mathrm{d}t \qquad (1)$$

where k_B is the Boltzmann constant and $\sigma_{\alpha\beta}$ can be any of the five independent anisotropic component of the stress tensor (e.g. σ_{xy}). An average over these five components is performed to improve the statistics. In practice, the value of the integral in Eq. 1 usually converges to a plateau in a few ps [33]. This allows to accumulate a reliable statistics using simulation runs of reasonable length (of

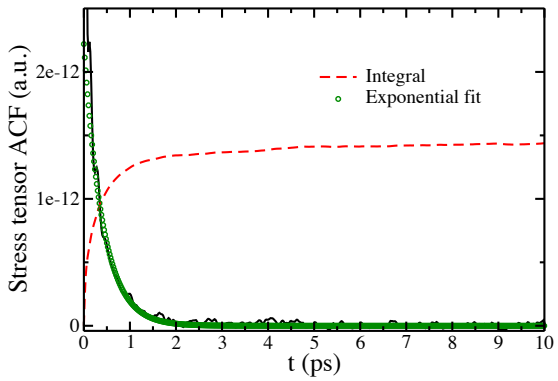

Fig. 3 Time evolution of the stress tensor correlation function in the system consisting in YCl_3-(LiCl-KCl)$_{eut}$ (x_{YCl_3}=0.1) at 1073 K. The viscosity is calculated from the plateau value of the integral.

the order of ns). An example of this running integral is shown in Figure 3. We also show a fit obtained by representing the stress-tensor correlation function as a decaying exponential

$$\langle \sigma_{\alpha\beta}(0)\sigma_{\alpha\beta}(t)\rangle \simeq A\exp\left(-t/\tau_M\right) \tag{2}$$

where τ_M is the Maxwell relaxation time, which we will discuss more fully below.

We show in Figure 4 the shear viscosity as a function of the MCl_3 mole fraction, for the four cases considered, $M^{3+} \equiv Y^{3+}$, Tb^{3+}, La^{3+}, U^{3+}. Although there is no experimental data for the compositions we simulate, we are confident on the predictive power of our polarisable force fields, which were validated against a wide range of experimentally available structural, thermodynamic and dynamical properties [8–13]. The temperature and concentration dependence of the Maxwell relaxation time τ_M follows that of the viscosity closely. We observe immediately the similarity in the behavior of the viscosity for the pairs of cations with similar ionic radii. At all temperatures, the viscosities for all metal cations at mole fractions $x_{MCl_3} = 0.1$ and 0.2 take very similar values and start to become significantly larger for La^{3+}/U^{3+} compared to Y^{3+}/Tb^{3+} by $x_{MCl_3} = 0.4$. Thereafter the viscosity increases with MCl_3 concentration more steeply for the larger cations. Finally, we can also see that, despite the very similar ionic radii of La^{3+} and U^{3+} (with Ka^{3+} slightly bigger), a significantly larger value of the viscosity is reached in $LaCl_3$-(LiCl-KCl)$_{eut}$, for which η at $T = 873$ K and x_{LaCl_3}=0.5 is about double that for the corresponding case in UCl_3-(LiCl-KCl)$_{eut}$.

Coordination numbers

We now move to the analysis of the structural properties of the systems in the hope of relating them to the behaviour of the viscosities. In Figure 1 we have already shown the M^{3+}-Cl^- RDFs at $T = 873$ K for the lowest, $x_{MCl_3} = 0.1$, and for the highest, $x_{MCl_3} = 0.5$, metal cation salt content. The behavior of the structure at the other two temperatures investigated, $T = 973$ K and $T = 1073$ K remains qualitatively similar. Furthermore we wanted to show the difference in

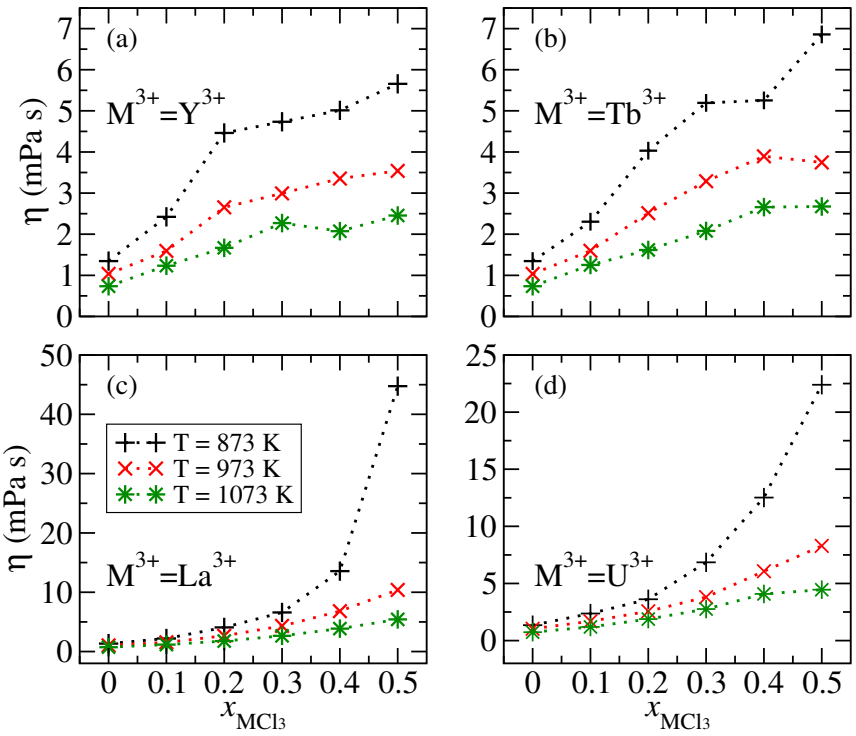

Fig. 4 Simulated shear viscosity η as a function of the MCl_3 mole fraction x_{MCl_3}. (a) $M^{3+} \equiv Y^{3+}$; (b) Tb^{3+}; (c) La^{3+}; (d) U^{3+}. The curves η vs. x_{MCl_3} are shown for the three temperatures investigated, $T = 873$ K (plus signs), $T = 973$ K (crosses) and $T = 1073$ K (stars). The dotted lines joining the points are guides for the eye. Note that $1\,\text{mPa}\cdot\text{s} = 1\,\text{cP}$.

the structure of the less and the most viscous systems, thus selecting the two extreme mole fractions. Before describing the details of the RDFs, we immediately note that for the structural properties, the similarity of the results for Y^{3+}/Tb^{3+} and the La^{3+}/U^{3+} pairings is already evident.

The sharp first peak in the RDF indicates a tight coordination complex and its position increases with the ionic radius of the cation M^{3+} as would be expected. In all cases, a decrease in the height of the first peak and of the depth of the first minimum is observed upon increasing the metal cation salt content. This indicates that when the mole fraction increases, the $M^{3+} - Cl^-$ coordination shell become less well defined. Also note that the first minimum of the $M^{3+} - Cl^-$ RDFs goes to zero only for Y^{3+}/Tb^{3+} at $x_{MCl_3} = 0.1$. In this case the $M^{3+} - Cl^-$ first coordination shell is then expected to remain stable on relatively long times, while in the other cases frequent exchanges of chloride anions are expected between the first and the second coordination shells of the cations.

The running integral of the M-Cl RDF out to the first minimum gives the average coordination number of the cation in that mixture; as we commented in the Introduction, this value was the focal point of many of the earlier structural studies. In the simulation we may examine the structure in more detail and, for each

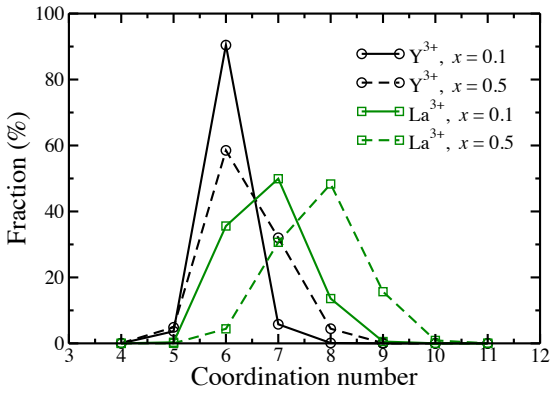

Fig. 5 The distribution of instantaneous coordination numbers in YCl_3 and $LaCl_3$ at the lowest and highest concentrations studied. The Y^{3+} distribution remains peaked at 6 across the concentration range, though it does broaden at higher concentrations. Even at the lowest concentration studied, the La^{3+} mean coordination number is larger than 6 and it shifts to still larger values at higher concentrations.

cation at each timestep, we may determine the number of anions within a spherical shell whose radius corresponds to the position of the minimum in the RDF and this constitutes an instantaneous coordination number for that cation. In Figure 5 we plot the distribution of these coordination numbers for Y^{3+} and La^{3+}, as representative of the small and large ions, at the two extreme concentrations and a temperature of 1073 K. We observe that, as anticipated in the Introduction, the width of these distributions narrows as the MCl_3 concentration is lowered into the dilute solution régime and that the mean of the distributions approaches 6. Elswehere it has been shown how an experimental observable, such as the EXAFS spectrum, may be regarded as a superposition of spectra associated with these different coordination complexes[13]. At higher concentrations, the distributions broaden but the mean coordination number for Y^{3+} remains close to 6, whereas that for La^{3+} begins to increase. In other studies[13,24] the mean coordination number in pure $LaCl_3$ has been found to be close to 8.

The viscosity and mean coordination number both increase with increasing MCl_3 concentration, the results are summarised in Figure 6. However, as we shall now demonstrate, this does not mean that the increase in coordination number should be seen as the *cause* of the rise in viscosity, rather that both are consequences of some other phenomenon affecting structure and dynamics.

Strength of the M-Cl ionic bonds

When the fluid is sheared it must relax to a new configuration and the timescale of this relaxation is the Maxwell relaxation time. Many types of microscopic events can contribute to this relaxation process and, in the present context, one might imagine that break-up of the M^{3+} coordination shells could be involved. We have therefore examined the strength of the M^{3+}-Cl^- linkages.

Although there is no established criterion to define the "strength" of an ionic bond, their stability may be estimated[36,37] by using the potential of mean force

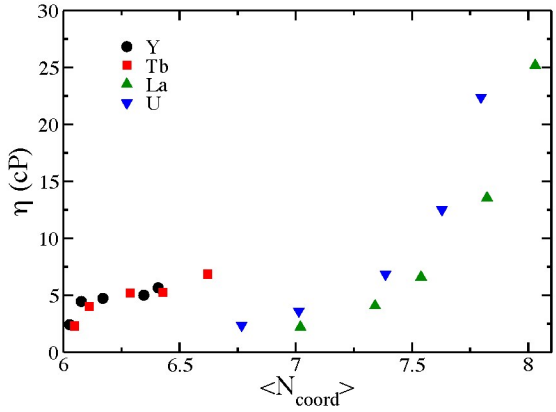

Fig. 6 The mean coordination number has been plotted against the viscosity for the different mixtures studied at 873 K.

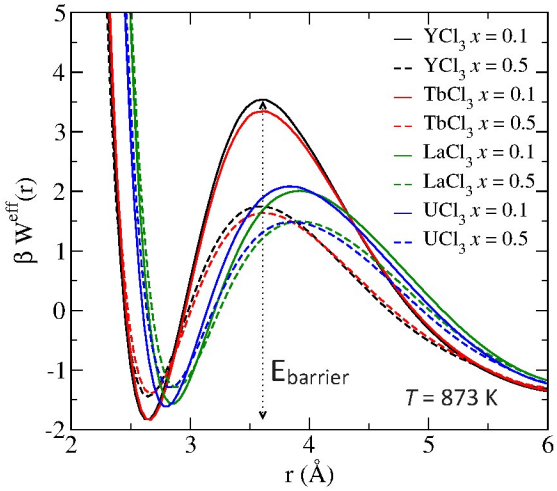

Fig. 7 The potential of mean force of mean force for the breaking of an M^{3+}-Cl^{-} "bond" in the various mixtures studied, at 873 K. Notice that the barrier to dissociation is higher for the smaller cations and that its height falls at increasing concentrations.

that determines the exchange of Cl^{-} with the first solvation shell of M^{3+} can be evaluated by

$$\beta W^{\mathrm{eff}}(r) = -\ln g_{\mathrm{M-Cl}}(r) - 2\ln\left(\frac{r}{r_{\mathrm{min}}}\right), \qquad (3)$$

where $\beta = 1/k_B T$ with k_B the Boltzmann constant and T the temperature of the simulation and r_{min} is a constant. These functions, shown on Figure 7, display a deep first minimum at the position of the first peak of the RDF. To escape this minimum, a coordinated Cl^{-} anion must overcome an energy barrier E_{barrier}.

Figure 8 indicates that the height of the barrier decreases with increasing concentration and with increasing coordination number, *i.e.* the opposite trend

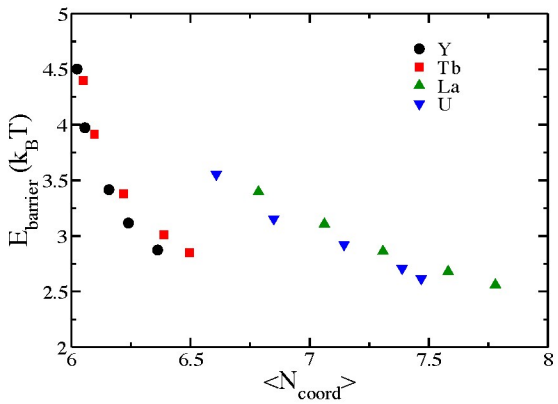

Fig. 8 The height of the barrier to dissociation is plotted *versus* the mean coordination number at 1073 K.

to the viscosity. This result is rather counter-intuitive since one may expect that stronger bonds will lead to a larger resistance to shear. We will return later to an explanation of why this trend arises.

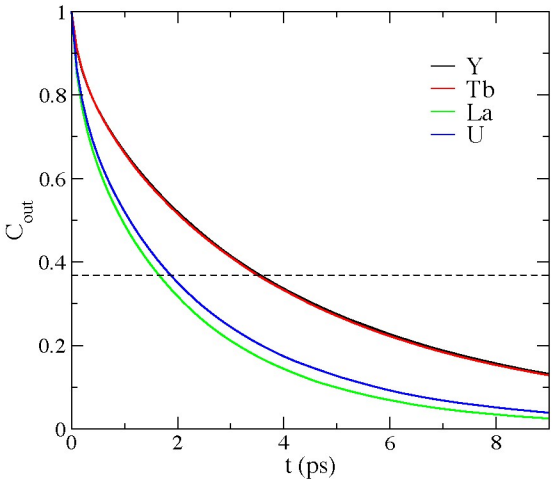

Fig. 9 Cage correlation functions for the cations of interest at a concentration of $x = 0.3$ and a temperature of 1073 K. Note that the relaxation times are longer for the smaller cations, in agremment with the expectation from the barrier heights in Figure 7.

As an alternative measure of the stability of the first coordination shell we analyze the rate of change of the instantaneous coordination number, which can be interpreted as the solvation shell lifetime. This is done by performing a cage correlation function analysis[33,38]. The first minimum of the M-Cl partial RDF is again used as a simple geometrical criterion to determine whether a chloride anion is located inside the first coordination shell of a cation at a given time. The number of counter-ions that have left the first coordination shell between time t to $t+\delta t$ is denoted $n_i^{out}(t, t+\delta t)$. The rate at which a single counterion (Cl^-)

leaves the M^{3+} ions solvation shell (the cage) is given by the cage-out correlation function[38], which is defined as:

$$C^{\text{out}}(t) = \frac{1}{N_{M^{3+}}} \left\langle \sum_{i=1}^{N_{Cl^-}} \Theta\left(1 - n_i^{\text{out}}(0,t)\right) \right\rangle, \tag{4}$$

where Θ is the Heaviside step function. Examples of cage correlation functions for the cations of interest at an MCl_3 concentration of 0.3 are shown in Figure 9. Note that the relaxation time is longer for the smaller cations indicating a greater degree of stability for the first coordination shell in these cases and in agreement with the trend in the barrier height for breaking of the M^{3+}-Cl bond.

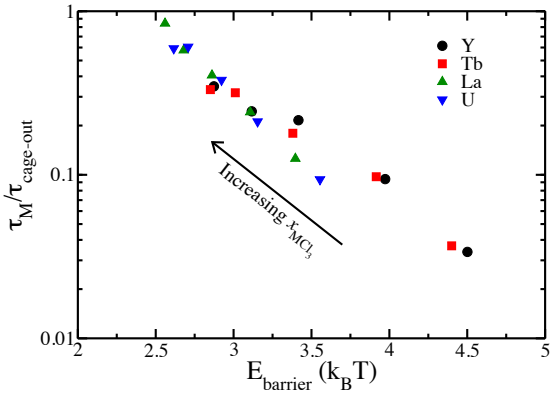

Fig. 10 The ratio of the cage and Maxwell relaxation times at 1073 K are plotted against the barrier heights determined above. Note that increasing barrier height is the direction of decreasing MCl_3 concentration.

In Figure 10 we have plotted the ratio of the Maxwell relaxation time to the cage correlation time against the barrier height for bond-breaking. The striking feature of the figure is that the cage relaxation time is much *longer* than the Maxwell time over most of the concentration range studied. In the relatively dilute solutions, then, the relaxation of the fluid to an applied shear is complete before the M^{3+} coordination shells have rearranged significantly - they behave as rigid units on the timescale of this relaxation. Only at the highest concentrations, where the fluid is becoming quite viscous due to the slow shear relaxation do the timescales become comparable. This confirms that to find a link between structure and the behaviour of the viscosity we will need to look beyond the first coordination shell.

Network forming ability

In contrast to the MCl RDFs, the M^{3+}-M^{3+} RDF for the larger and smaller cations differ markedly. In Figure 11(a) we show the $Y^{3+} - Y^{3+}$ RDFs and in Figure 11(b) we show those for $La^{3+} - La^{3+}$. The temperature considered here is always $T = 873$ K and as previously the behavior for $Tb^{3+} - Tb^{3+}$ is qualitatively analogous to the one for $Y^{3+} - Y^{3+}$, while the behavior for $U^{3+} - U^{3+}$ is similar to the one for $La^{3+} - La^{3+}$, so these two cases are not shown for clarity.

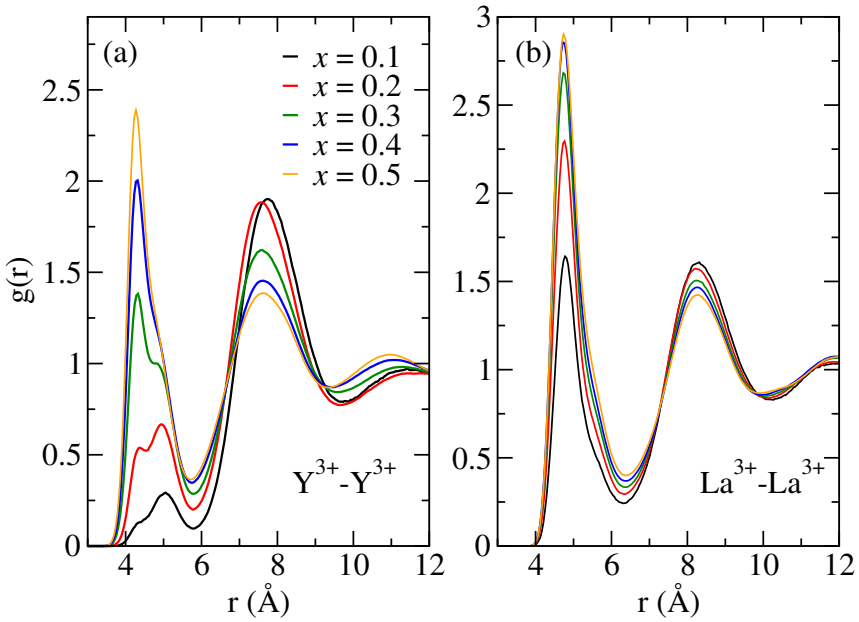

Fig. 11 RDFs for the pairs (a) $Y^{3+} - Y^{3+}$; (b) $La^{3+} - La^{3+}$ at $T = 873$ K and for all the span of the MCl_3 mole fractions investigated. The features appearing at small $r < 6$Åarise from pairs of cations with overlapping coordination shells.

If we focus, initially, on the Y-Y case for the most dilute $x = 0.1$ concentration we see a small feature, composed of two partially merged peaks, at small Y-Y separations ($r \sim 5$Å) and a much larger peak at $r \sim 8$Å. Recalling that the most probable Y-Cl separation for the first coordination shell is (from Figure 1) $r_{M-Cl} \sim 2.7$Å we can associate the first feature with pairs of cations with overlapping coordination shells. At this low concentration, the probability that a neighbouring pair of cations are involved in such an association is much smaller than if they are unassociated (recall that the probability of being associated with a given RDF peak is proportional to the integral of r^2 times the RDF over the peak, so that one needs to notionally treble the area of the peak at larger r relative to the first to gain an estimate of the ratio of probabilities). Thus, to a first approximation, in this dilute case, the yttrium melt may be viewed as solution of separated YCl_6^{3-} ions dispersed in the solvent. We will see shortly that the double-peaked nature of the first feature arises from the presence of Y-Y pairs which share a single anion or two anions in their coordination shells, corresponding to the corner- and edge-sharing linkages illustrated in Figure 2. The latter are associated with the peak at smaller r in the $r \sim 5$Å in the RDF. As the concentration of YCl_3 in the mixture increases we see that the probability that a Y^{3+} ion is involved in these Cl-bridged linkages with neighbouring Y^{3+} ions increases dramatically. From a direct examination of the instantaneous configurations generated in the simulations we may classify the M-M linkages depending on the number of anions that the two cations share and count the corner-sharing, edge-sharing and face-sharing (three common anions) MCl_n polyhedra[39]. By

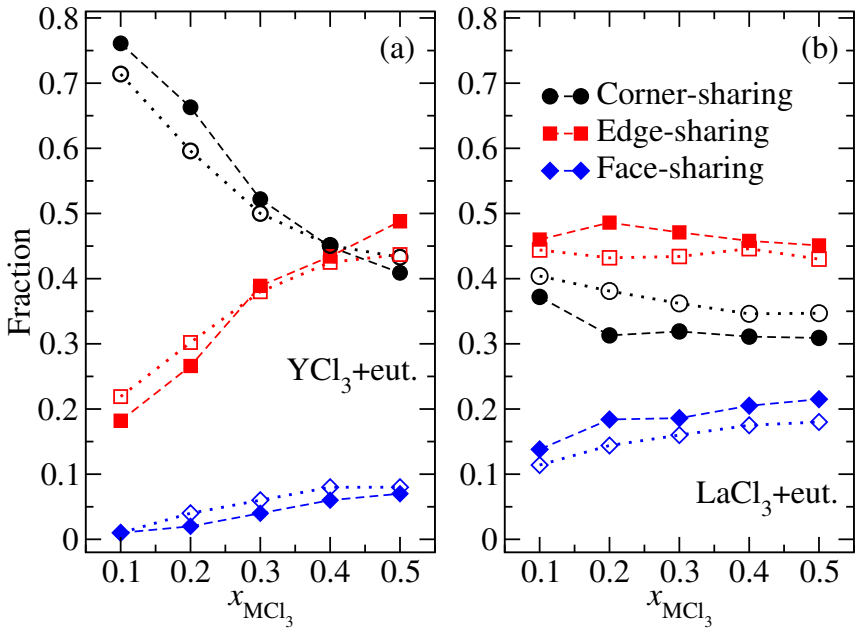

Fig. 12 Analysis of the number of anions shared between two M^{3+} cations within first shell distances. One anion indicates a corner–sharing configuration, two cations an edge–sharing configuration and three cations a face–sharing configuration. The analysis is shown for the case of (a) $YCl_3-(LiCl--KCl)_{eut}$; (b) $LaCl_3-(LiCl-KCl)_{eut}$. The values showed are for $T = 873$ K (solid symbols) and for $T = 1073$ K (hollow symbols). At all temperatures and at all MCl_3 mole fractions, the fraction of cases when the $M^{3+}-Cl^-$ pair is not connected to another M^{3+} is about 0.05 for YCl_3 and about 0.03 for $LaCl_3$ (not shown for clarity).

performing this analysis, we obtain a majority of corner-sharing species, and a minority of edge-sharing species at low YCl_3 concentrations, as shown on Figure 12. For the largest concentrations in YCl_3, although we observe an increase of both peaks, the short-distance (edge-sharing) one grows more rapidly and becomes predominant by $x = 0.5$. We note the formation of a few face-sharing species, although no characteristic peak is observed for them in the RDFs.

The $La^{3+}-La^{3+}$ case behaves quite differently. Firstly, the intensity of the low r peak is considerably larger than for YCl_3 mixtures, and implies a significant degree of cross-linking even at the lowest concentrations studied. From the linkage analysis in Figure 12 we observe that the three types (corner, edge and face) of sharing coexist, and that the variations of their relative extent is much smaller than in the case of Y^{3+}. Secondly, the first peak in the RDF is not split in the manner of the Y-Y case. However, by examining it more carefully, we can see the first peak is quite asymmetric, and we can attribute the shoulder on its right side to the corner-sharing configurations. The implication is that the M-M separation for corner- and edge-sharing configurations is smaller for La-La than Y-Y, and simply not resolved.

The proportion of M^{3+}-Cl^- bonds involved in these linkages becomes quite

high, linking the cations into a network (as visualised in Figure 2). We can illustrate this with a simple analysis for the Y^{3+} case, where the coordination number remains close to 6 across the concentration range. For the $x = 0.5$ concentration, the stoichiometry dictates that there are 4 Cl^- ions per Y^{3+} and, counting a Cl^- involved in a linkage as contributing one half to each cation, we see that to complete the coordination shell of a cation 4 out of the 6 anions there must be involved in linkages to other cations. We can now see a reason why the barriers to dissociation and the lifetimes of the M^{3+}-Cl^- bonds decrease with increasing coordination. The measures we have used to characterise the strengths of these bonds average over all the M^{3+}-Cl^- bonds in the system and therefore increasingly reflect the characteristics of the shared linkages at higher concentrations. We can also see that the tendency to increased coordination with increasing coordination must be linked to the propensity to form linkages of different types.

At $x = 0.5$ we see from Figure 12 that the proportions of corner- and edge-shared linkages between Y^{3+} ions are roughly equal and, for ease of this simplified discussion, we will ignore the small number of face-sharing cases. Since the edge-sharing links account for two of the four anions in the coordination shell involved in linkages we can expect that (on average) each Y^{3+} is participating in two corner-sharing linkages and one edge-sharing one and therefore is connected to three other Y^{3+} cations. This degree of connectedness is sufficient to cause the cations to be considered linked into an extended network. Note too that, depending on the types of linkages formed (corners *vs.* edge *vs.* face) the number of cations linked to a given cation will vary and we should expect this to influence the character of the network and its strength, and we note the different proportions exhibited by the small and larger cations in our study (figure 12). Wilson[39,40] has discussed the relationship between fluidity and the concept of network connectivity in tetrahedrally-coordinated glass-formers[41,42]. In the field of amorphous solids a critical coordination number above 2.4 at the vertices of the network is signalling the transition to a rigid state and Wilson has examined whether the same analysis can be applied to measures of fluidity in the liquid.

4 Discussion: cross-linking, network-structure and the viscosity

The picture which has emerged from the above analyses is of an increasing degree of cross-linking between the cations as the concentration is increased and the emergence of a network. The challenge now is to link the properties of the network to the rapid increase in the viscosity at higher concentrations, with a view to pointing to reasons why, for example, the La/U-containing melts are more viscous than the Y/Tb ones at higher concentrations.

An analogous challenge was to account for the very strong concentration dependence of the viscosity in mixture of BeF_2 with LiF - an important component of many proposed molten salt nuclear reactors[1]. In these systems the Be^{2+} ions are invariably tetrahedrally coordinated to four F^- and, whilst present as isolated BeF_4^{2-} ions at low concentrations, become increasing linked by bridging F^- ions in exclusively corner-sharing arrangements as the concentration is increased[8,9,43,44]. As the concentration approaches the equimolar point, the viscosity increases sharply and becomes very high for pure BeF_2 - which is a good

glass-forming material (unlike the pure MCl_3 systems). Although there are numerous differences in the structure compared to the MCl_3 (well-defined 4-coordinate, only corner-sharing linkages) the relationship between the local dynamics of bond-breaking and the viscous relaxation is very similar to that exposed above for the MCl_3:ACl mixtures[45].

In particular, at low concentrations, where the highly charged cations are involved in simple BeF_4^{2-} or YCl_6^{3-} units or small oligomers of them, these units behave as rigid bodies on the timescale of viscous relaxation, which is dominated by solvent relaxation, and the cage relaxation time is much longer than the Maxwell time. As the concentration reaches the point where the degree of cross-linking between cations becomes large enough to support an extended network (the speciation of Be-containing ions was followed explicitly in the BeF_2 case) the viscosity increases markedly and the cage relaxation time becomes much more similar to the Maxwell time (quantitatively in the $LaCl_3$ case and in exhibiting the same concentration dependence in BeF_2). These similarities support the assertion that the viscous relaxation at higher concentrations is dominated by the reorganisation of the network in the MCl_3 mixtures. In the BeF_2 case, we showed that the Be-F cage time becomes a good measure of the timescale for breaking the Be-Be links in the network. We also showed that this latter timescale increased as the network became more complete at higher concentrations and suggested that this was because the constraints imposed by the surrounding network inhibited the breaking of the linkage - so that the individual links stiffen as the network becomes more extended.

Despite these similarities, there are significant differences in the behaviour of the viscosity between the BeF_2 and the MCl_3 cases with the former becoming far more viscous. This may simply be a consequence of the greater strength of the Be-F bond, but may also reflect the differences in local and network structure. The MCl_3 systems exhibit a much higher mean coordination number and a more flexible coordination shell and several different (corner, edge and face sharing) types of intercation linkages - all of which suggest that other types of local reorganisation than the simple breaking of M-Cl bonds may be possible and allow the network configuration to relax. Wilson[39,40] has shown that the breaking of an edge-sharing linkage is substantially slower than a corner-sharing one, which suggests that the presence of edge- and face-sharing linkages will stiffen the network; however, as noted above they also reduce the number of cations to which a given cation is linked, and hence also reduce the connectedness of the network. It is likely that a further examination of these factors will be necessary to fully explain the difference in behaviour of the viscosity of YCl_3 and $LaCl_3$.

Acknowledgements

This work was carried out with the European Commission financial support in the 7th framework program, under the collaborative project “SACSESS”, Grant Agreement No. 323282.

References

1 C. Le Brun, *J. Nucl. Mater.*, 2007, **360**, 1–5.

2 T. Kato, T. Inoue, T. Iwai and Y. Arai, *J. Nucl. Mater.*, 2006, **357**, 105–114.
3 J. J. Katz, G. T. Seaborg and L. R. Morss, *The Chemistry of Actinide Elements (II ed.)*, Chapman and Hall, New York, 1986, vol. 1.
4 H. On Nam and D. Morgan, *J. Nucl. Mater.*, 2015, **465**, 224–235.
5 K. Grjotheim, C. Krohn, M. Malinovsky, K. Matiasovsky and J. Thonstad, *Fundamentals of the Hall-Héroult Process*, Aluminium-Verlag, Dusseldorf, Germany, 1982.
6 P. A. Madden and M. Wilson, *Chem. Soc. Rev.*, 1996, **25**, 339.
7 M. Salanne and P. A. Madden, *Mol. Phys.*, 2011, **109**, 2299–2315.
8 R. J. Heaton, R. Brookes, P. A. Madden, M. Salanne, C. Simon and P. Turq, *J. Phys. Chem. B*, 2006, **110**, 11454–11460.
9 M. Salanne, C. Simon, P. Turq, R. J. Heaton and P. A. Madden, *J. Phys. Chem. B*, 2006, **110**, 11461–11467.
10 M. Salanne, C. Simon, P. Turq and P. A. Madden, *J. Phys. Chem. B*, 2008, **112**, 1177–1183.
11 F. Hutchinson, M. Wilson and P. A. Madden, *Mol. Phys.*, 2001, **99**, 811–824.
12 Y. Okamoto, P. Madden and K. Minato, *J. Nucl. Mater.*, 2005, **344**, 109–114.
13 Y. Okamoto, S. Suzuki, H. Shiwaku, A. Ikeda-Ohno, T. Yaita and P. A. Madden, *J. Phys. Chem. A*, 2010, **114**, 4664–4671.
14 M. Rovere and M. P. Tosi, *Rep. Prog. Phys.*, 1986, **49**, 1001–1081.
15 M. P. Tosi, D. L. Price and M.-L. Saboungi, *Annu. Rev. Phys. Chem.*, 1993, **44**, 173.
16 A.-L. Rollet and M. Salanne, *Annu. Rep. Prog. Chem., Sect. C*, 2011, **107**, 88–123.
17 G. M. Photiadis, B. Borresen and G. N. Papatheodorou, *J. Chem. Soc., Faraday Trans.*, 1998, **94**, 2605–2613.
18 G. A. Voyiatzis, A. G. Kalampounias and G. N. Papatheodorou, *Phys. Chem. Chem. Phys.*, 1999, **1**, 4797–4803.
19 G. D. Zissi and G. N. Papatheodorou, *Phys. Chem. Chem. Phys.*, 2004, **6**, 4480–4489.
20 *X-Ray Diffraction Analysis of Ionic Liquids (Molten Salt Forum, vol. 3)*, ed. H. Ohno, K. Igarashi, N. Umesaki and K. Furukawa, Trans Tech Publications, Switzerland, 1994.
21 J. C. Wasse and P. S. Salmon, *J. Phys.: Condens. Matter*, 1999, **11**, 1381–1396.
22 J. C. Wasse and P. S. Salmon, *J. Phys.: Condens. Matter*, 1999, **11**, 9293–9302.
23 H. E. Fischer, A. C. Barnes and P. S. Salmon, *Rep. Prog. Phys.*, 2006, **69**, 233–299.
24 W. J. Glover and P. A. Madden, *J. Chem. Phys.*, 2004, **121**, 7293–7303.
25 E. Robert, J. E. Olsen, V. Danek, E. Tixhon, T. Ostvold and B. Gilbert, *J. Phys. Chem. B*, 1997, **101**, 9447–9457.
26 B. Gilbert, E. Robert, E. Tixhon, J. Olsen and T. Ostvold, *Inorg. Chem.*, 1996, **35**, 4198–4210.
27 E. Robert, V. Lacassagne, C. Bessada, D. Massiot, B. Gilbert and J. Coutures, *Inorg. Chem.*, 1999, **38**, 214–217.
28 V. Lacassagne, C. Bessada, P. Florian, S. Bouvet, B. Ollivier, J.-P. Coutures and D. Massiot, *J. Phys. Chem. B*, 2002, **106**, 1862–1868.
29 Z. Akdeniz and P. A. Madden, *J. Phys. Chem. B*, 2006, **110**, 6683–6691.
30 S. Cikit, Z. Akdeniz and P. A. Madden, *J. Phys. Chem. B*, 2014, **118**, 1064–1070.
31 R. D. Shannon, *Acta Cryst.*, 1976, **A32**, 751–767.
32 A. S. Basin, A. B. Kaplun, A. B. Meshalkin and N. F. Uvarov, *Russ. J. Inorg. Chem.*, 2008, **53**, 1509–1511.
33 R. Brookes, A. Davies, G. Ketwaroo and P. A. Madden, *J. Phys. Chem. B*, 2005, **109**, 6485–6490.
34 K. Fukasawa, A. Uehara, T. Nagai, N. Sato, T. Fujii and H. Yamana, *J. Nucl. Mater.*, 2012, **424**, 17–22.
35 M. Salanne, B. Rotenberg, C. Simon, S. Jahn, R. Vuilleumier and P. A. Madden, *Theor. Chem. Acc.*, 2012, **131**, 1143.
36 O. Pauvert, M. Salanne, D. Zanghi, C. Simon, S. Reguer, D. Thiaudière, Y. Okamoto, H. Matsuura and C. Bessada, *J. Phys. Chem. B*, 2011, **115**, 9160–9167.
37 M. Levesque, V. Sarou-Kanian, M. Salanne, M. Gobet, H. Groult, C. Bessada and A.-L. Rollet, *J. Chem. Phys.*, 2013, **138**, 184503.
38 E. Rabani, J. D. Gezelter and B. J. Berne, *J. Chem. Phys.*, 1997, **107**, 6867–6876.
39 M. Wilson, *Phys. Chem. Chem. Phys.*, 2012, **14**, 12701–12714.
40 M. Wilson, *J. Phys.: Condens. Matter*, 2012, **24**, 284114.
41 M. Thorpe, *J. Non-Cryst. Solids*, 1983, **57**, 355–370.

42 M. Bauchy and M. Micoulaut, *EPL*, 2013, **104**, 56002.
43 J. Dai, D. Long, P. Huai and Q. Li, *J. Mol. Liq.*, 2015, **211**, 747–753.
44 J. Dai, H. Han, Q. Li and P. Huai, *J. Mol. Liq.*, 2016, **213**, 17–22.
45 M. Salanne, C. Simon, P. Turq and P. A. Madden, *J. Phys. Chem. B*, 2007, **111**, 4678–4684.